energies

MDPI

Article

Biomass Fast Pyrolysis Vapor Upgrading over γ-Alumina, Hydrotalcite, Dolomite and Effect of Na_2CO_3 Loading: A Pyro Probe GCMS Study

Harsha Mysore Prabhakara *, Eddy A. Bramer and Gerrit Brem

Department of Thermal and Fluid Engineering, University of Twente, 7500 AE Enschede, The Netherlands; e.a.bramer@utwente.nl (E.A.B.); g.brem@utwente.nl (G.B.)

* Correspondence: h.mysoreprabhakara@utwente.nl; Tel.: +31-53-489-7469

Abstract: The influence of γ-alumina, hydrotalcite, dolomite and Na_2CO_3 loaded γ-alumina, hydrotalcite, dolomite on fast pyrolysis vapor upgrading of beechwood was investigated using an analytical pyro probe-gas chromatography/mass spectrometry instrument (Py-GC/MS) at a temperature of 500 °C. Overall, this research showcased that these catalysts can deoxygenate biomass pyrolysis vapors into a mixture of intermediate compounds which have substantially lower oxygen content. The intermediate compounds are deemed to be suitable for downstream hydrodeoxygenation processes and it also means that hydrogen consumption will be reduced as a result of moderate in-situ deoxygenation. Among the support catalysts, the application of hydrotalcite yielded the best results with the formation of moderately deoxygenated compounds such as light phenols, mono-oxy ketones, light furans and hydrocarbons with a TIC area % of 7.5, 44.8, 9.8 and 9.8, respectively. In addition, acids were considerably reduced. Dolomite was the next most effective catalyst as γ-alumina retained most of the acids and other oxygenates. Na_2CO_3 loading on γ-alumina had a noticeable effect on eliminating more or less all the acids, enhancing the mono-oxy-ketones and producing lighter furans. In contrast, Na_2CO_3 loading on dolomite and hydrotalcite did not show a major impact on the composition except for further enhancing the mono-oxy-ketones (e.g., acetone and cyclopentenones). Additionally, in the case of hydrotalcite and γ-alumina, Na_2CO_3 loading suppressed the formation of hydrocarbons. In this research, the composition of pyrolytic vapors as a result of catalysis is elaborated further under the specific oxygenate groups such as acids, phenolics, furanics, ketones and acids. Further the catalysts were also characterized by BET, XRD and TGA analysis.

Keywords: deoxygenation; dolomite; hydrotalcite; sodium carbonate; pyroprobe

Citation: Mysore Prabhakara, H.; Bramer, E.A.; Brem, G. Biomass Fast Pyrolysis Vapor Upgrading over γ-Alumina, Hydrotalcite, Dolomite and Effect of Na_2CO_3 Loading: A Pyro Probe GCMS Study. *Energies* **2021**, *14*, 5397. https://doi.org/10.3390/en14175397

Academic Editor: Dmitri A. Bulushev

Received: 24 July 2021
Accepted: 26 August 2021
Published: 30 August 2021

1. Introduction

Ever-increasing global demand for energy supply and potential climate change adversities due to unwarranted usage of fossil fuels have resulted in an increased focus on bio-based fuels, chemicals and heat and power [1,2]. In this context, lignocellulosic biomass which is a 2nd generation biomass feedstock has gained momentum as a prospective carbon-neutral feed material for the generation of biofuels and bio chemicals via appropriate technologies [3]. In general, technologies based on biochemical or thermo-chemical pathways have been investigated considerably [4]. Fermentation, digestion and enzymatic hydrolysis are some established biochemical routes. Ethanol and methanol are deemed to be the most salient liquid biofuels generated via these routes [5]. Pyrolysis, gasification, combustion and hydrothermal carbonization are some established thermochemical approaches for transforming biomass to useful fuels and chemicals [4]. Techno-economic evaluations have suggested that the fuels for mobility and transport are

economically viable when produced via the fast pyrolysis of biomass in comparison to biochemical alternatives due to their flexibility in feeds and products [6]. In fast pyrolysis, feedstock is swiftly heated to a temperature of around 450–550 °C in an atmosphere containing inter gas. During this time, the biomass decomposes to char, combustible gases and pyrolysis oil vapors. These vapors are quickly quenched to prevent secondary cracking to chars and gases, thereby maximizing the yield of pyrolysis oil up to 75% in mass [7]. However, the direct application of produced pyrolytic oil is limited due to its acidic, corrosive, viscous and unstable characteristics. These characteristics stem from a high concentration of highly oxygenated compounds [8].

Deoxygenation of pyrolysis vapors can be accomplished via the application of catalysts in the process. In general, catalysts can be introduced into the process as a mixture with the biomass in the reactor (in situ operation) or can be placed separately in a downstream process (ex situ operation). Dehydration, decarboxylation, decarbonylation, cracking, aromatization, cyclization and alkylation are some typical competing reactions which occur as a result of catalysis. As a result, products of the thermal decomposition are transformed ideally into alkanes and mono-aromatics, which are commonly found in fossil-based fuels. The great advantage of this process is that it can be done under atmospheric pressure and no external H_2 is required to produce a higher quality product [9].

Zeolite Y, Beta, Mordenite, ZSM-5 and HZSM-5 are among the most widely evaluated in-situ catalysts for the pyrolysis vapor upgrading. Among these zeolites, HZSM-5 has shown promising results in lowering the oxygenates and increasing the desired aromatic hydrocarbons in pyrolysis biooil. This effect has been mainly attributed to shape selectivity, unique three-dimensional microporous structure and density of acid sites [10–13]. However, this upgradation comes with loss of oil yield as these catalysts favor deoxygenation in the form of H_2O and CO, which is less energetic compared to oxygen removal as CO_2. The deoxygenation pathway should be selective enough to minimize the carbon loss and retain the hydrogen. Oxygen removal in the form of CO and H_2O is a lost potential to generate hydrogen, which can be utilized to remove oxygen further. Moreover, the high rate of coking and thus the tendency to deactivate more rapidly has hindered its application at an industrial scale [14].

Beside zeolites, metal oxides like ZnO, MgO, CaO, Fe_2O_3, and ZrO/TiO_2 have received considerable attention and there are substantial indications in effectively deoxygenating the pyrolysis vapors [15–19], respectively. Also, waste stream such as bauxite processing waste was investigated as a catalyst and the higher heating value of the bio-oil was upgraded to a value 29.46 MJ/kg [20]. Nevertheless, [21–23] reported that 20% wt.% Na_2CO_3 supported on γ-Al_2O_3 can yield a bio-oil containing lesser oxygen functionalities, which result in a heating value very comparable to that of fossil fuels. However, the application of this catalyst drastically decreased the bio-oil yield to as low as 9 wt.% and resulted in formation of oxygen-containing carbonyls. This necessitates a downstream hydrodeoxygenation process where hydrogen is required. The source of hydrogen is a very critical factor in determining the sustainability of such a process. The required hydrogen can be acquired sustainably via externally and/or internal routes. External processes such as steam reforming of methane, heavy oil oxidation, thermochemical decomposition of water, steam gasification of coal and biomass can provide hydrogen [24]. To reduce the requirement of H_2 from external sources, the catalysts must be selected on the basis of their ability to deoxygenate and also produce in situ H_2 [25]. One way is to introduce catalysts which can capture CO_2 to shift the equilibrium of the water gas shift reaction towards hydrogen production.

Dolomite is one such catalyst which has yielded a pyrolysis oil with moderately improved properties and also produced a H_2 enhanced gas as a result of CO_2 capture [26,27]. Similarly, dolomite has also been applied as a tar reforming catalyst [28] in biomass gasification to enhance H_2 in syngas. Further, Na_2CO_3-loaded calcium oxide (CaO) showed increased capacity for CO_2 sorption in a study by C.H. Lee et al., 2018 [29]. In addition, hydrotalcite (HTC), which has a structure similar to that of the hydrotalcite mineral

($Mg_6Al_2(OH)_{16}CO_3{\cdot}4H_2O$), has been investigated as a catalyst in transesterification, C-C bond forming reactions and as a CO_2 sorbent [30–32], respectively. HTC is also of interest as it is known to be resistant to biomass-derived sulphur gases such as H_2S [33]. Acid and base sites on hydrotalcite make them attractive for investigation in biomass catalytic pyrolysis [34]. Further Na_2CO_3-promoted HTC has shown to enhance the CO_2 sorption capacity compared to HTC [35]. Nevertheless, a lack of data exits on hydrotalcite, dolomite and the effect of Na_2CO_3 loading in pyrolysis conditions.

Therefore, this research is aimed at exploring the potential of hydrotalcite and dolomite in deoxygenating biomass pyrolysis vapors. Subsequently, 20 wt.% Na_2CO_3 was also loaded on hydrotalcite and dolomite to explore for its effect on biomass pyrolysis vapors. Further, γ-Al_2O_3 and 20 wt.% Na_2CO_3/γ-Al_2O_3 were also studied to provide a comparative analysis. To achieve this, small amounts of biomass mixed with catalyst were pyrolyzed using a Py-GC/MS instrument. Experiments were carried out at a temperature of 500 °C and the influence of catalysts on the composition of the pyrolytic products was analyzed qualitatively.

2. Materials and Methods

2.1. Biomass

A commercially available beechwood sawdust in the tradename Lignocel® HBS 150–500 was supplied by J. Rettenmaier and Söhne GmbH for the experiments. Particle size was in the range of 0.15 to 0.5 mm. The samples were dried at 105 °C for 24 h and then stored in a desiccator. Table 1 shows the condensed ultimate and proximate analysis of the dried beech wood. Elemental analysis of beechwood was done according to ASTM D5291-16 by using an Inter-science Flash 2000 elemental analyzer. Mass fraction of oxygen was calculated by difference. Sulphur content was not measured in the setup used, however beechwood generally contains around 0.02 wt.% sulphur [36]. The proximate analysis was conducted on a TA instruments Q5500 TGA with initially heating up the biomass at the rate of 10 °C/min under nitrogen flow and in the temperature range of 30–950 °C. Furthermore, the nitrogen was switched to air to oxidize of the fixed carbon and then the residual mass represented the ash content.

Table 1. Ultimate and Proximate Analysis.

Ultimate Analysis (wt.% Dry Basis)				Proximate Analysis (wt.% Dry Basis)		
C	**H**	**N**	**O** [a]	**Volatiles**	**Fixed Carbon**	**Ash**
48.7	6.1	0.1	45.1	84.87	14.53	0.59

[a] by difference

2.2. Catalyst Preparation

The catalysts were obtained as follows. Dolomite from Omya, Hydrotalcite (HTC) MG70 pellets from Sasol and γ-Alumina pellets from Alfa Aesar. These catalysts are referred to as catalyst supports in this work. Sodium carbonate (Na_2CO_3, ACS reagent grade >99.5%) was procured from Sigma-Aldrich. In general, all the catalysts were characterized as follows. Thermogravimetric analysis (TGA) was performed on a TA instruments Q5500 TGA to determine the thermal decomposition patterns of catalysts. The analysis was performed under flowing nitrogen atmosphere in the temperature range of 30–950 °C with the heating rate of 10 °C/min. X-Ray diffractometer (XRD) analysis was done on a Bruker D2 Phaser XRD device using Cu Kα1 radiation source. Diffractograms were recorded over the range 2θ = 10–80°, scanning rate of 1°/min and with a step size of 0.05°. Surface characteristics of the catalysts were measured using N_2 adsorption-desorption isotherms at 77 K by employing a Micromeritics ASAP 2400 instrument. The surface area was calculated by the application of the BET equation; the surface of the micropores was obtained by applying the t-plot method; BJH calculations were applied for obtaining pore size distribution and average pore diameter.

2.2.1. 20 wt.% Na_2CO_3/γ-Alumina Impregnation

Extrudates of γ-Alumina were downsized to 300 to 400 microns prior to wet impregnation. In the procedure of impregnation as followed by [22], the required amount of a precursor was dissolved in water and subsequently added to the support (H_2O/support = 5 *w*/*w*). The obtained slurry was mixed for 2 h and then dried in an oven at 105 °C. The catalyst was then calcined at 550 °C for 10 h under ambient air.

2.2.2. 20 wt.% Na_2CO_3/HTC-MG70 Impregnation

The received calcined HTC-MG70 pellets were downsized to 300 to 400 microns prior to Na_2CO_3 impregnation. The impregnation method as described by [35] was employed in this research. HTC-MG70 was soaked in an Na_2CO_3 solution containing the required amount of precursor. The obtained slurry was dried at 110 °C under vacuum and subsequently grounded and sieved to a size of 300 to 400 μm. The sample was calcined in static air at 550 °C overnight.

2.2.3. 20 wt.% Na_2CO_3/Dolomite Impregnation

The received dolomite particles were sieved to particle sizes 300 to 400 μm and then calcined in static air for 4 h at 800 °C to obtain CaO and MgO phases. The calcined dolomite was then impregnated in the Na_2CO_3 solution under the magnetic stirring for 4 h. The obtained slurry was then vacuum filtered and dried at 105 °C overnight and then sieved to 300 to 400 μm. Finally, the dried catalyst was calcined at 800 °C overnight.

2.3. Fast Pyrolysis Analysis (Py-GC/MS)

Pyro probe is an analytical equipment integrating an analytical pyrolyser with a GC/MS and it has been applied frequently to explore the influence of different mixtures of biomass streams and catalysts undergoing catalytic fast pyrolysis. It enables the user to quantify the pyrolysis products very rapidly. In this investigation, a CDS pyro-probe 5000 series (CDS Analytical, Inc.) coupled to a GC/MS system (6890N Network GC System, 5975B inert XL MSD, Agilent Technologies) equipped with a 60 m VF-1701ms (0.25 μm) column Agilent J&W Technologies) was used to conduct the experiments. Pyrolysis experiments were carried out by introducing approximately 1 mg of beechwood supported by minor amounts of quartz wool on both sides into the quartz tube. To explore the effect of different catalysts, biomass was physically mixed with the catalyst and was then loaded into the quartz tube and also supported by quartz wool in a similar fashion. The catalyst-to-biomass ratio (C/B) was varied until there were no significant changes detected in the composition of vapors for different catalysts studied here.

The biomass or biomass/catalyst sample were pyrolyzed with a heating rate of 20 °C/ms at a temperature of 500 °C. Subsequently, the evolving pyrolysis vapors were rapidly mixed with helium carrier gas in the pyrolyser interface and transferred into the GC/MS for identification. For effective separation of the evolving components as a result of pyrolysis, the oven temperature was programmed to 40 °C for 5 min and then ramped up to 280 °C at 3 °C/min and was kept isothermal for 10 min using Helium as carrier gas. The flowrate of Helium gas was 1.2 mL/min in split mode 100:1. The GC/MS interface temperature was held isothermally at 300°. The ion source temperature, and the auxiliary heater temperature of the mass spectrometer were maintained 230 and 270 °C, respectively. The mass spectra were obtained in the range of m/z ratio between 35–400 amu. The GC/MS was operated in the electron ionisation (EI) mode.

Experiments were repeated twice to make certain the reproducibility. The detection of evolving compounds as a result of catalytic pyrolysis were accomplished by comparing the mass spectra of the chromatographic peaks with standard spectra from the National Institute of Standards and Technology NIST library. GC/MS technique is known to be limited in extracting a quantitative analysis of the compounds. Therefore, in this analysis it was assumed that the chromatographic peak area percentage of a volatile compound is

proportional to its concentration by a 1st order approximation as the amount of beechwood was always the same. The evaluation of the change in relative yield of compounds obtained from different experiments was done by comparing corresponding chromatographic peak area percentages. Also, the summation of the peak areas of the chromatograms were within the same order of magnitude for all the experiments. In order to decipher the influence of the various catalysts on the composition of the products, all the detected compounds were classified based on oxygen functionalities. These included acids, aldehydes, anhydro-sugars, ketones, furans, phenols, hydrocarbons, alcohols and nitrogen-containing compounds. Further, minor unidentifiable peaks were put together as others.

3. Results

3.1. Catalyst Characterization

Both support catalysts and Na_2CO_3-loaded catalysts were characterized by TGA, BET and XRD analysis. The following sections aim to discuss the results of these analyses.

3.1.1. Thermogravimetry Analysis

The thermal decomposition profiles of the catalysts (without any biomass) were obtained on a TGA analyzer as depicted in Figure 1a–c. The foremost mass loss for the γ-alumina occurred at ~105 °C, which can be credited to the absorbed moisture. Further, the mass continued to decrease with increasing temperature, which can be linked to dehydration reactions accompanied by phase changes [37]. The Na_2CO_3-impregnated γ-Al2O3 showed three additional decomposition peaks in addition to moisture removal at ~265 °C, and ~705 °C and ~849 °C. These peaks are ascribed to the decomposition of various sodium compounds on the γ-alumina surface [38].

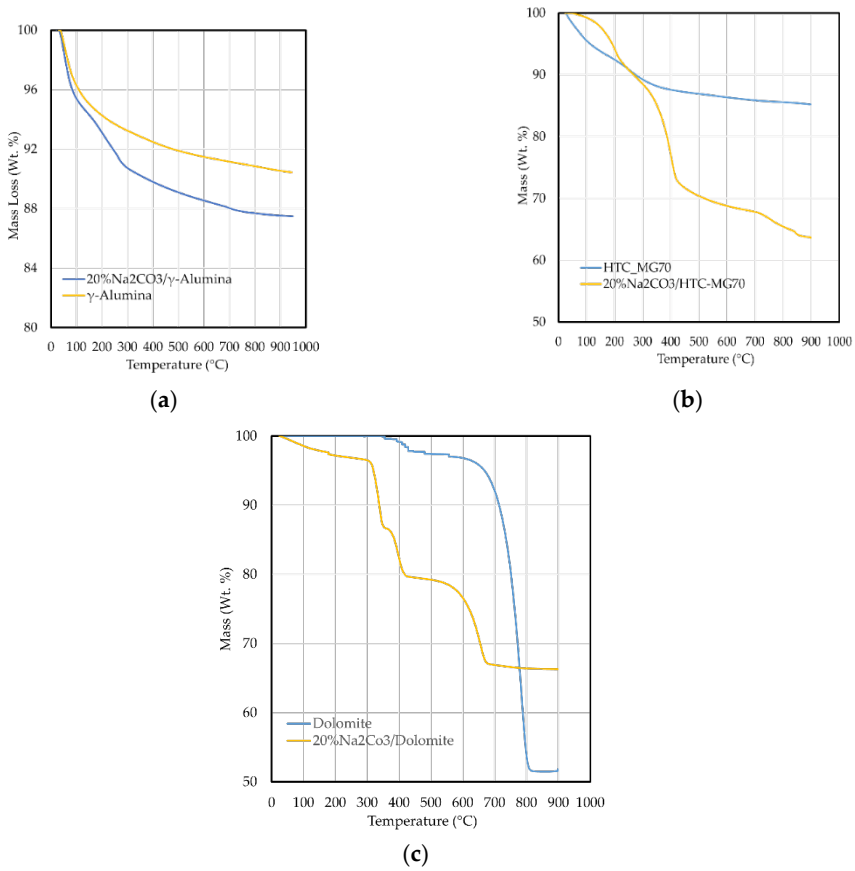

Figure 1. The Thermogravimetric Analysis (**a**) γ-Alumina and 20%Na_2CO_3/γ-Alumina. (**b**) HTC-MG70 20%Na_2CO_3/HTC-MG70 (**c**) Dolomite and 20%Na_2CO_3/Dolomite.

HTC-MG70 was calcined by the supplier at 550 °C. Generally, when the hydrotalcites are heat treated above 350 °C, their structure collapses due to dehydration and decomposition of anions in the interlayer spaces. This results in the formation of Mg-Al mixed oxides. In Figure 1b it can see that the mass loss is around 12% up to a temperature of 900 °C after the calcination step by the supplier. This loss can be attributed to physically observed moisture and dihydroxylation of the remaining hydroxyl groups and decarbonation of carbonate groups. In contrast, the thermal decomposition of the Na_2CO_3/HTC-MG70 occurred via four successive weight loss steps. The initial mass loss was observed in the range of 50–250 °C and it is attributed to the removal of water absorbed on the surface of the catalyst and the interlayers. This amounted to 8% of the original weight. The next mass loss step was in the temperature range from 250 to 425 °C. This loss corresponds to the dihydroxylation of the OH groups, which are linked with the Al^{3+} and Mg^{2+} ions in the brucite layers. Subsequently, at temperatures higher than 425 °C, carbonate anions linked to the cations in the inter-laminar spaces were eliminated. The final step was deemed to happen when the strongly combined carbonate in the LDH decomposed. The weight loss at 850 °C possibly corresponds to the melting of Na_2CO_3 but is not certain as the gas products were not analyzed.

The thermal decomposition profile of the as received dolomite is shown in Figure 1c and it revealed that the decomposition mainly took place in the temperature range of 425–800 °C. This is ascribed to direct transformation of calcium magnesium carbonate into CaO and MgO. In contrast, there were three weight losses when Na_2CO_3 was loaded on calcined dolomite. The first weight loss corresponds to the evaporation of adsorbed water and decomposition of $Mg(OH)_2$ to MgO (30 to 350 °C). The second weight loss is due to dehydroxylation of $Ca(OH)_2$ between temperatures 350 and 410 °C. Finally, the decomposition of weakly bonded carbonates on Ca or Mg species occurred up to a temperature of 700 °C.

3.1.2. Surface Morphology

The change in the crystal structure due to Na_2CO_3 loading was analyzed with the XRD spectra, as seen in Figure 2a–c. The crystalline properties of commercial γ-alumina and 20% Na_2CO_3/γ-alumina are shown by the XRD pattern in Figure 2a. XRD analysis of γ-alumina revealed three wide peaks at 2θ of 38°, 46° and 66°, which correspond to the (311), (400) and (440) planes are observed. All the diffraction peaks seem to have acquired a high magnitude of broadness. This can be generally explained by the fine nature of nano-sized crystalline domains along with a few imperfections. Sharp crystalline peaks corresponding sodium compounds were not observed. As a result, it can be ascertained from the analysis that sodium carbonate was dispersed uniformly as small clusters on γ-alumina.

The XRD pattern of HTC-MG70 showed prevailing peaks at 2θ = 35.3°, 43.3°, and 63°. These peaks are characteristic of halite structure MgO with low crystallinity. It is the MgO segregated from an amorphous Mg-Al oxide matrix. When HTC-MG70 was loaded with Na_2CO_3, the crystal structure of Na_2CO_3 was revealed in the XRD pattern, as seen in Figure 2b. Interestingly, even after Na_2CO_3 loading, the characteristic peaks of HTC-MG70 were detected without any distinguishable shift. This implied that Na_2CO_3 was added without drastically changing the HTC-MG70 double-layered structure.

The XRD pattern of the calcined dolomite showed the diffraction peaks ascribed to the revenant of calcium oxide (CaO) at 2θ = 37.6° and magnesium oxide (MgO) at 2θ = 43.2°. Peaks corresponding to calcium magnesium carbonate $CaMg(CO_3)_2$ were not revealed by the XRD analysis and thus confirmed the calcination process. Even after Na_2CO_3 impregnation on calcined dolomite, the peaks of CaO and MgO were still dominant without any distinguishable shift. Therefore, it could be possible for Na_2CO_3 to be dispersed on the surface of dolomite. Further, it can also be seen as crystallinity loss of Na_2CO_3 as a result of exceeding the Tamman temperature during calcination.

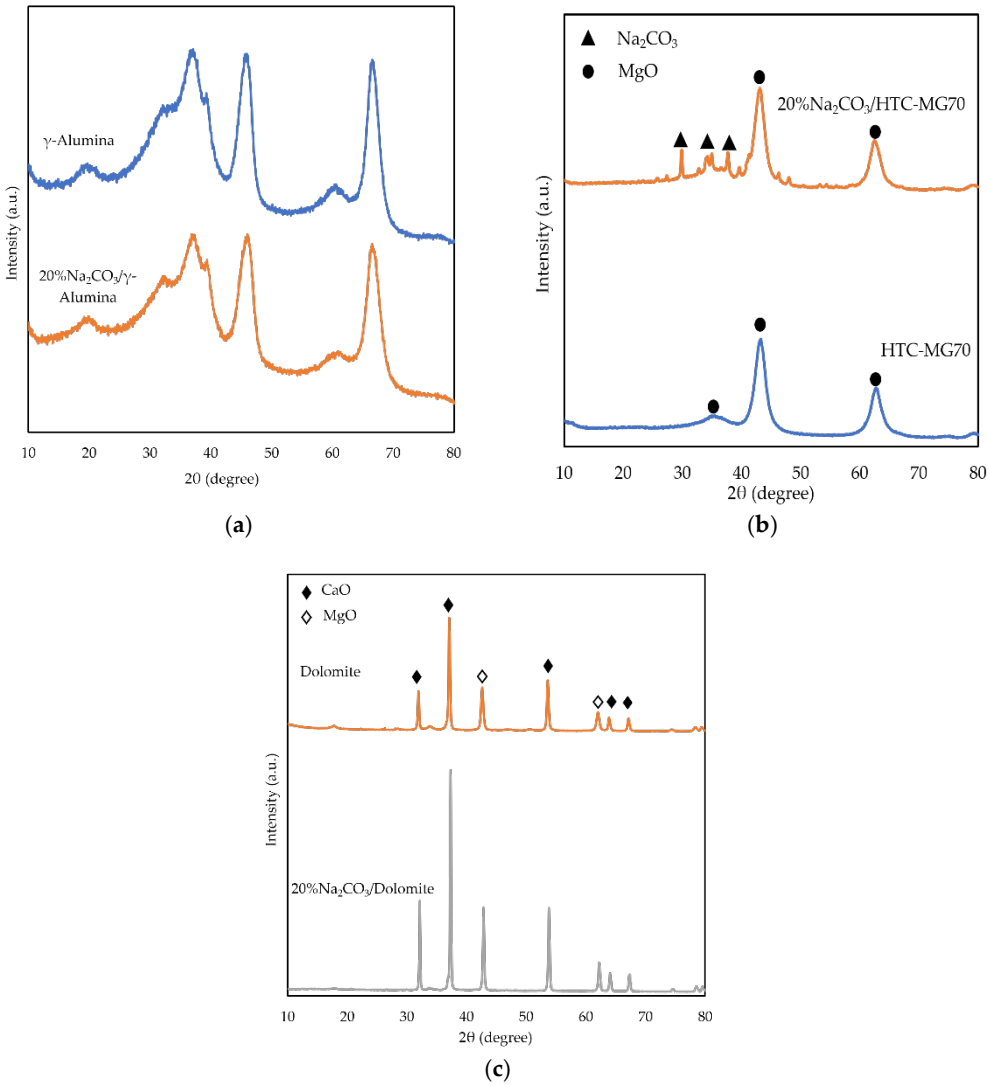

Figure 2. XRD patterns of (**a**) γ-Alumina and 20%Na_2CO_3/γ-Alumina (**b**) HTC-MG70 20%Na_2CO_3/HTC-MG70 (**c**) Dolomite and 20%Na_2CO_3/Dolomite.

Table 2 lists the textural properties of samples which include the surface area, average pore size, and the pore volumes. The surface area and pore volume of all samples decreased after Na_2CO_3 impregnation. This can be explained by the blockage of small pores by Na_2CO_3.

Table 2. Specific Surface Areas.

Sl. No.	Sample	Surface Area S_{BET} (m^2/g)	Pore Diameter D_p (nm)	Micro Pore Volume (cm^3/g)	Total Pore Volume V_p (cm^3/g)
1	Dolomite	27	40	0.001	0.1
2	HTC-MG70	168	5	-	0.3
3	γ-Alumina	262	10	0.006	0.8
4	20%Na_2CO_3/Dolomite	7.8	75	-	-
5	20%Na_2CO_3/HTC-MG70	152	7	-	0.2
6	20%Na_2CO_3/γ-Alumina	242	8	0.008	0.7

3.2. Influence of Catalysts on the Transformation of Pyrolytic Products

The influence of γ-Alumina, hydrotalcite (HTC)-MG70 and dolomite were investigated on the in-situ reforming of beechwood pyrolysis vapors. The influence of Na_2CO_3 loading on these support catalysts was also investigated. The distribution of products grouped according to their dominant functionalities is presented in Figure 3a,b. The analysis of the non-catalytic TIC revealed that the phenols were the most abundant group (41.76%) followed by ketones (22.52%), furans (7.17%) and alcohols (6.82%). Specifically, a mixture of multifunctional oxygenates such as 2-Propanone-1-hydroxy, Furfural, 3-ethyl-2-hydroxy-Phenol and 2-methoxy-4-(1-propenyl)-, (E)-, etc., were produced.

The application of γ-Alumina, HTC-MG70 and dolomite decreased the yields of phenols and acids, while it increased the yields of hydrocarbon, ketones, aldehydes and furans. Other product groups such as alcohols, anhydro-sugars and N-compounds showed very minor fluctuations in their relative yields. In general, the trends were similar for all the support catalysts, as shown in Figure 3a. Further, Na_2CO_3 loading altered the relative yields of products. Compared to γ-Alumina, 20%Na_2CO_3/γ-Alumina yielded less aromatics and furans, while it further increased the ketones (e.g., acetone and cyclopentenones). It also more or less eliminated the acids. Compared to HTC-MG70, 20%Na_2CO_3/HTC-MG70 reduced the relative yields of hydrocarbons, while it increased the formation of ketones. Compared to dolomite, 20%Na_2CO_3/dolomite enhanced the ketones and furans. Relative yields of hydrocarbons remained more or less the same in Figure 3b. In order to elaborate further on the results, specific groups of pyrolytic products such as ketones, acids, furans, hydrocarbons and phenols are discussed in the following sections. In the start of each section, the effect of the support catalyst on each specific group is discussed and further the effect of Na_2CO_3 loading is discussed.

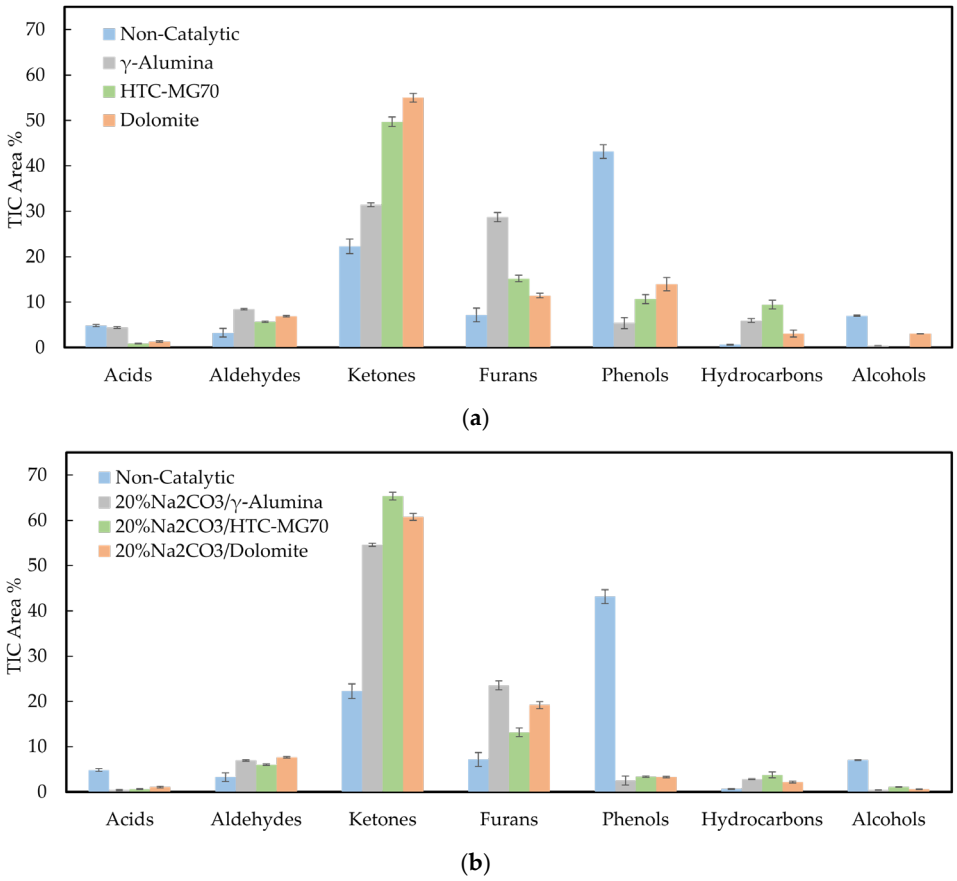

Figure 3. Overall Product Distribution—(**a**) support catalysts (**b**) Na_2CO_3-loaded support catalysts.

3.2.1. Acids and Aldehydes

It is well known that acids and aldehydes negatively influence the characteristics of bio-oils [39]. For example, the acids in pyrolysis oil can lead to problems during utilization in combustion engines owing to corrosion. In this investigation, acetic acid and 4-hydroxy-3-methoxy-benzoic acid were the primary acidic products detected. Acetic acid is predominantly derived from the rupture of acetyl groups bonded to the backbone of hemicellulose polysaccharides during fast pyrolysis [40]. The use of dolomite and hydrotalcite considerably minimized the relative acid yields as shown in Figure 4a. This could be due to the catalytic cracking ability and/or basicity of these catalysts. Research has shown that acids can be converted via Ketonization to form ketones on active basic sites of calcium-based catalysts [16]. In contrast, γ-alumina barely affected the yield of acids. Nevertheless, when Na_2CO_3 was loaded on γ-alumina, it more or less eliminated the acids as shown in Figure 4b. In contrast, Na_2CO_3 loaded on hydrotalcite and dolomite did not show any significant changes. However, the literature has shown alkali metal carbonates loaded on hydrotalcites (HT`s) to be effective in neutralizing acidic vegetable oils to produce biodiesel [41].

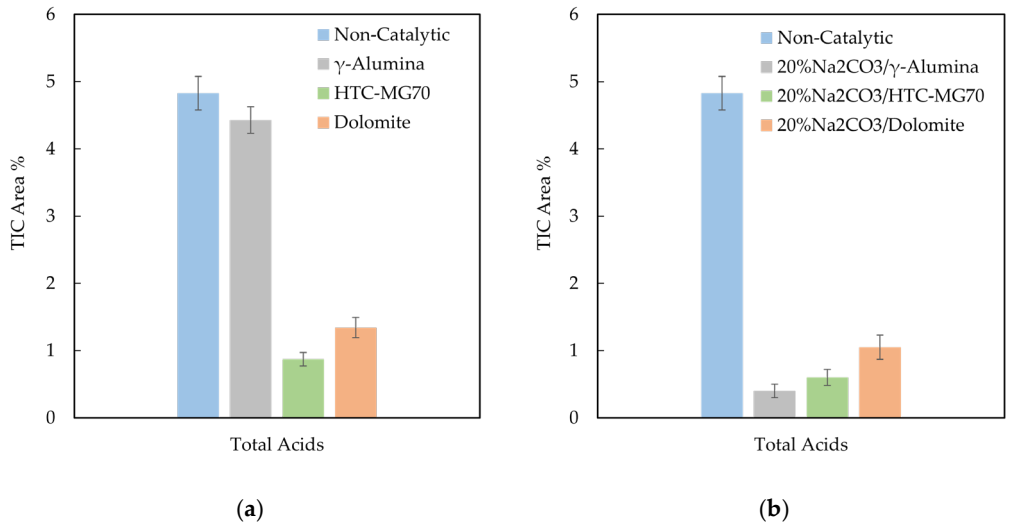

Figure 4. Effect of (**a**) support catalysts and (**b**) Na_2CO_3-loaded catalyst on acids.

The relative yield of the linear aldehydes such as acetaldehyde and butanedial were enhanced as a result of γ-alumina, hydrotalcite and dolomite catalysis. This indicated that the pyrolytic ring scission and reforming reaction pathway were dominant during the primary decomposition of cellulose and xylan. These reactions are known to be initiated inside the polysaccharidic monomers, which result in such small volatile compounds [42,43]. Besides that, the yields of benzene-containing aldehyde compounds such as benzaldehyde and 4-Hydroxy-2-methoxybenaldehyde remained more or less unaffected by catalysis. This suggests that decarbonylation on the aromatic ring was not promoted. The loading of Na_2CO_3 also resulted in a similar composition.

3.2.2. Alcohols and Anhydro-Sugars

Both linear and benzene-containing OH functionalities were detected during beechwood pyrolysis. The yield of 5-tert-Butylpyrogallol was most abundant and with the application of dolomite, its yield was reduced by almost 50%. This suggests that dolomite was effective in cracking high oxygen-containing benzene-diols. Furthermore, the Na_2CO_3 loading on dolomite further enhanced the cracking, resulting in complete elimination. In contrast, γ-alumina and hydrotalcite eliminated the 5-tert-Butylpyrogallol without the need for Na_2CO_3 loading. Further, the yield of anhydro sugars such as levoglucosan was

also completely eliminated both with the application of support catalysts and Na_2CO_3 loading. This substantiates that these catalysts promoted pyrolytic ring scission and the reforming reaction pathway and not the depolymerization reaction through trans glycosylation.

3.2.3. Ketones

For the purpose of further analysis, the ketonic compounds were divided into two subgroups: 1) linear ketones and their derivatives containing oxygen functional groups such as hydroxy, 2) cyclic ketones and their derivatives containing methyl-substitution and/or hydroxy-methyl substitution. Figure 5a,b showcases the overall distribution of linear and cyclic ketones for support catalysts and Na_2CO_3-loaded support catalysts, respectively.

The data revealed that the relative yield of ketones drastically increased from 22.28% up to 31.43%, 49.71% and 55% in the presence γ-alumina, hydrotalcite and dolomite, respectively, as shown in Figure 5a. Hydrotalcite and dolomite catalysis enhanced the formation of linear ketones. The major linear ketones identified were acetone, 2,3-butanedione, and 3-hexanone. The increase in the formation of C5 and C6 ketones indicate aldol condensation reactions being promoted as a result of the basic sites hydrotalcite and dolomite. For example, investigation by Mante et al., 2015 [44] attributed the increase in C5 and C6 ketones to strong basic sites of CaO. In contrast, γ-alumina did not enhance the formation of linear ketones. Nevertheless, Na_2CO_3 loading further increased the formation of linear ketones to 54.57%, 65.34% and 60.75% for γ-alumina, hydrotalcite and dolomite, respectively, as shown in in Figure 5b. This is a direct result of increased basicity of the catalyst.

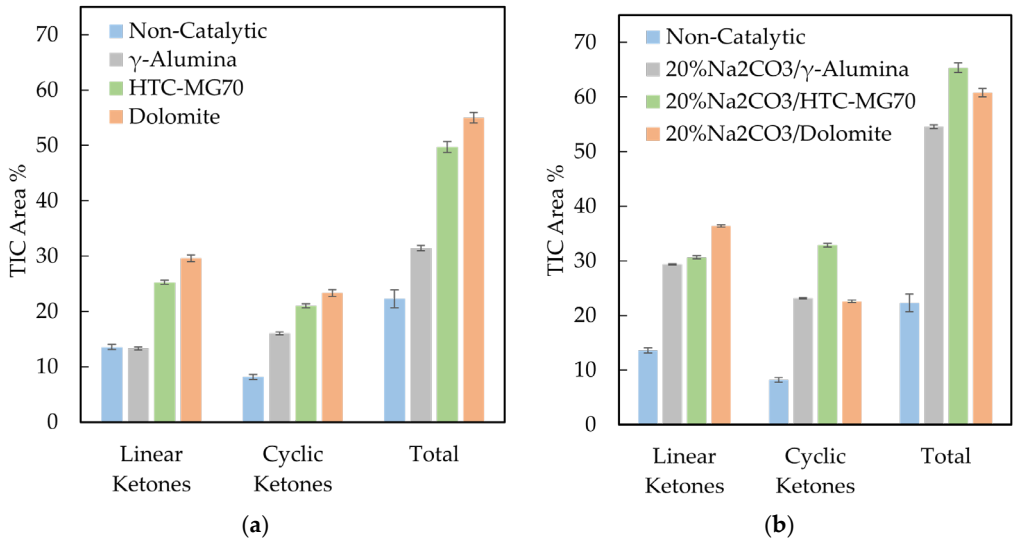

Figure 5. Distribution of ketones (**a**) support catalysts (**b**) Na_2CO_3-loaded support catalysts.

Further, the relative yields of cyclic ketones such cyclopentanones were enhanced by the addition of γ-alumina, hydrotalcite and dolomite. In general, cyclopentanones are products of cellulose and hemicellulose dehydration [45] and therefore it can be stated that these catalysts promoted dehydration reactions during pyrolysis. For example, such products were also enhanced when calcium-based catalysts were employed for catalytic pyrolysis of pine wood and polar wood, respectively [18,26]. On the contrary, Na_2CO_3 loading further enhanced the formation of linear ketones to 54.57%, 65.34% and 60.75% for γ-alumina, hydrotalcite and dolomite, respectively, as shown in in Figure 5b. Further analysis revealed that hydroxy-substituted 2-cyclopentenones were reduced, while the abundance of methyl-2-cyclopentenones increased for both support and Na_2CO_3-loaded

catalysts, as seen in Figure 6a,b. This indicates that these catalysts promoted the dihydroxylation/side chain cracking reaction in linear and cyclic ketones and thus yielded monooxy functional ketones with reduced oxygen contents.

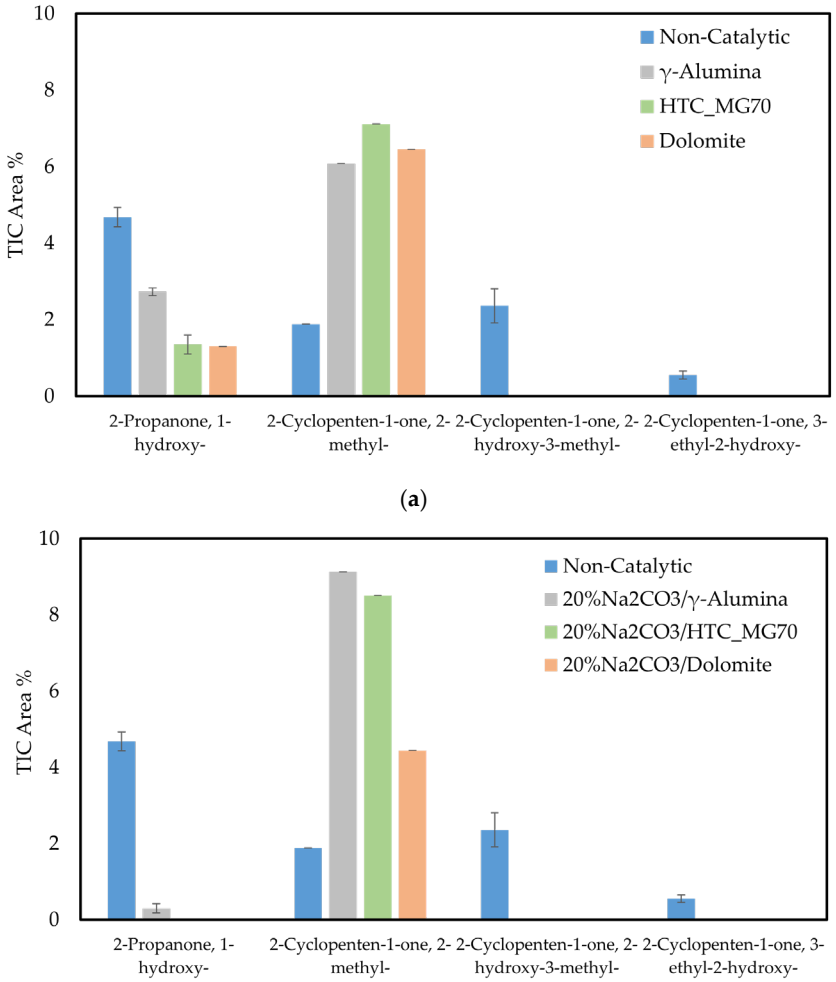

Figure 6. (**a**) Effect of support catalysts. (**b**) Effect of Na_2CO_3 loading on major cyclic-Ketones.

3.2.4. Hydrocarbons

Hydrocarbons enhance the higher heating value of the bio-oil and thus it is beneficial to promote the formation of hydrocarbons. Figure 7a,b shows the effect of support catalyst and Na_2CO_3 loading on the hydrocarbons. For the purpose of analysis, the hydrocarbons were grouped into (1) Aliphatic, (2) Mono-Aromatics and (3) Poly Aromatics. The fast pyrolysis of beechwood generated a very limited amounts of hydrocarbons. The application of γ-alumina, hydrotalcite and dolomite increased the hydrocarbon yield from 0.65% to 5.96%, 9.48% and 3.09%, respectively.

γ-alumina promoted the formation of hydrocarbons, but the extent of aromatic production was limited. Hydrotalcite was the most active in the forming of both aliphatic and aromatic compounds. Among the aromatics, it showed selectivity towards Benzene and Indene derivatives. This can probably be explained by the synergy between Bronsted and Lewis acid sites. Dolomite was least effective in promoting hydrocarbon formation. However, methylated aliphatic compounds such as 2,4-Hexadiene, 2,3-dimethyl-, 4-Methyl-1,3-heptadiene, 2,4-Hexadiene, 2,3-dimethyl-were formed probably as a result of cracking of high-molecular-weight compounds. In the case of γ-alumina and hydrotalcite, the acidic nature resulted in enhancement of hydrocarbon production compared to dolomite.

On the other hand, the Na_2CO_3 loading on γ-alumina and hydrotalcite suppressed the formation of hydrocarbons to a great extent. The relative yields decreased to 2.80% and 3.75% from 5.96% and 9.48% for Na_2CO_3-loaded γ-alumina and hydrotalcite, respectively. This result can be explained of decreased acidity of these catalysts. Hydrocarbon formation via Na_2CO_3-loaded dolomite remained more or less the same as compared to dolomite.

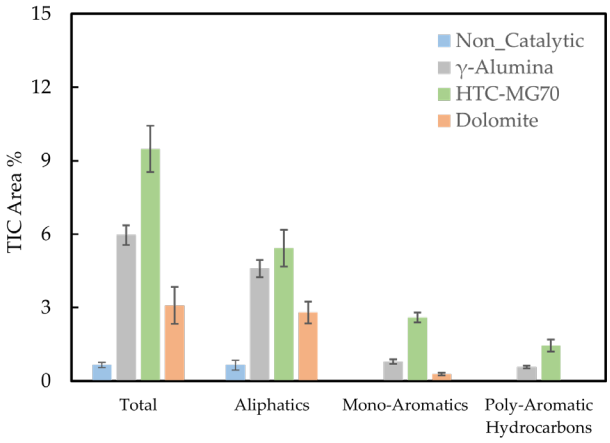

(**a**)

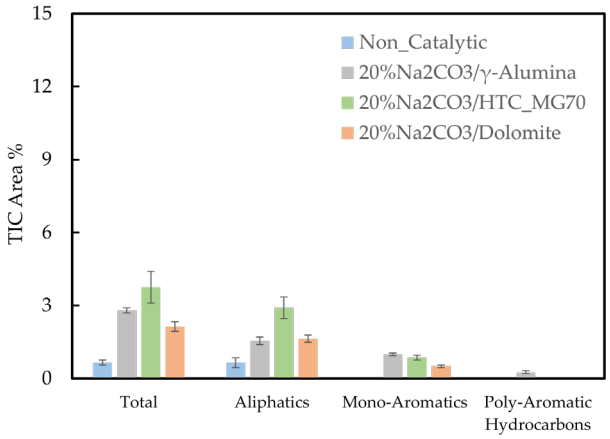

(**b**)

Figure 7. (**a**) Effect of support catalysts. (**b**) Effect of Na_2CO_3 loading on hydrocarbons.

3.2.5. Furanics

During pyrolysis, furanic compounds are formed due to depolymerization reactions through the glycosidic bond rupture of holocellulose [46]. The thermal pyrolysis is mainly composed of furfural. The application of γ-alumina, hydrotalcite and dolomite enhanced the furanic yield from 7.17% up to 28.74%, 15.20% and 11.45%, respectively. In the case of hydrotalcite and dolomite, the yields of furan and furan 2-methyl increased, while the yield of furfural decreased, as shown in Figure 8a. This indicates that these catalysts promoted the rupture of C-O and C-C bonds in furfural. Moreover, hydrotalcite and dolomite showed selectivity towards the formation of furan methanol, which suggests the promotion of a hydrogenation reaction. γ-alumina showed higher selectivity to form furanic compounds in comparison to hydrotalcite and dolomite. However, γ-alumina enhanced the formation of both furan and furfural. This can be explained by the presence of acidic sites on γ-alumina which are known to catalyze dehydration of holocellulose into furfurals. In addition, γ-alumina also showed tendencies to form Benzo-Furans. Overall, this

demonstrated that dolomite and hydrotalcite were more effective in transforming high oxygen-containing furfural towards lighter furanic compounds such as furans.

On the other hand, Na_2CO_3 loading on γ-alumina reduced the yields of furanic compounds from 28.74% to 23.53%. Yields of furan, furan 2-methyl, furfural and benzo-furans reduced due to reduced acidity of γ-alumina. However, the overall composition remained similar. Further, Na_2CO_3 loading on hydrotalcite only slightly reduced the yields of furanic compounds from 15.20% to 13.17% and the composition of furanic compounds remained more or less the same. In contrast, Na_2CO_3 loading on dolomite enhanced the rupture of C-O and C-C bonds in furfural leading to enhanced yields of furans and furan-2-methyl. The relative yield increased from 11.45% to 19.17%. All the relative yields were still above the non-catalytic experiments.

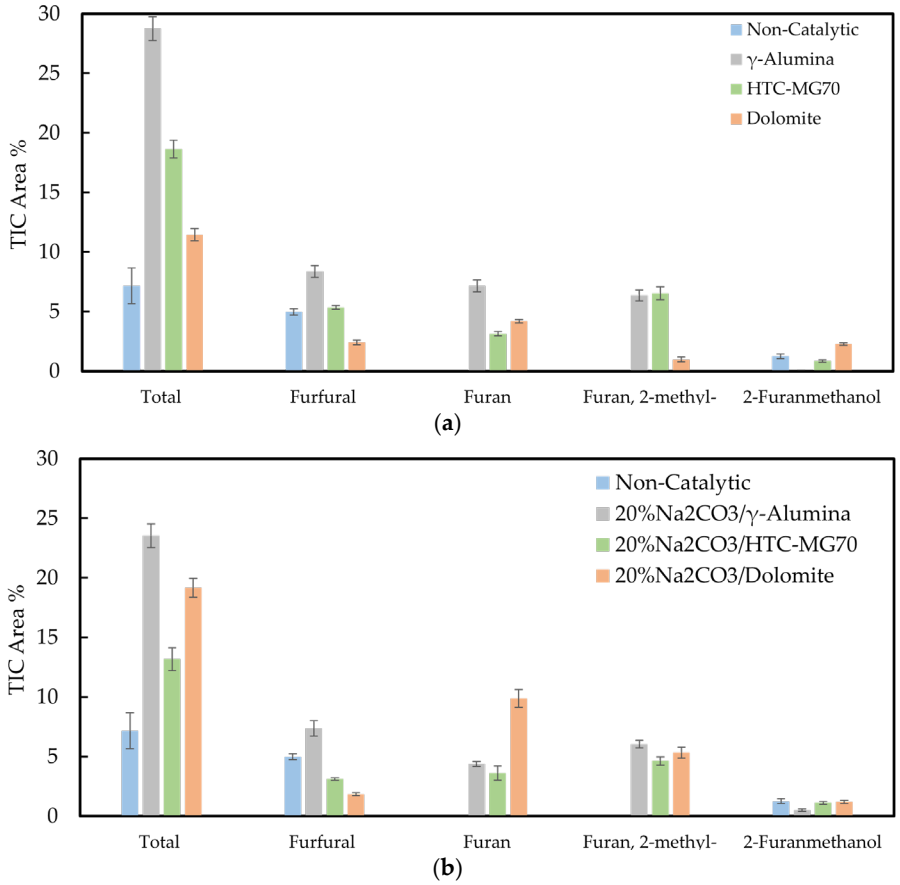

Figure 8. Effect of (**a**) support catalysts (**b**) Na_2CO_3-loaded catalysts on Furanics.

3.2.6. Phenolics

Monomeric and oligomeric phenolic compounds are mainly a result of pyrolytic decomposition of lignin in the biomass [47]. They are undesirable in pyrolysis oil due to their influence on instability and viscosity and thus removal of these compounds is a general aim of any upgrading process. Figure 9a,b depicts the effect of the support catalyst and Na_2CO_3 support catalysts on the phenolic compounds, respectively. The application of γ-alumina, hydrotalcite and dolomite reduced the phenolic yield from 43.15% to 5.48%, 10.68% and 13.94%, respectively. Therefore, it is very likely that application of catalysts converted phenolics to other products or even promoted polymerization reactions to form cokes/chars. For a much deeper insight and further analysis, phenolic compounds were classified as lighter phenols (e.g., Phenol and Cresols) and heavier phenols (e.g., Guaiacol, Creosol, Syringol and Eugenol) based on the functional groups present. The lighter phenols are free of a methoxyl group on the aromatic ring and additionally they are free of

unsaturated C-C bonds on the side chain. On the contrary, heavier phenols have unsaturated C-C bonds on the side chain and/or methoxyl group.

Non-catalytic experiments mainly produced heavy phenols such as Syringol and Eugenol. Analysis of the catalytic experimental data revealed that the lighter phenols were enhanced, while the heavy phenols were reduced to a great extent for support catalysts. More specifically, hydrotalcite yielded the lightest phenols. Significant reduction in the phenol yield by the application of γ-alumina indicated both deoxygenation of heavy phenols in addition to coking reactions. This transformation of heavy phenols to light phenols is beneficial, as heavy phenols have higher oxygen content. Na_2CO_3 loading was effective in reducing the heavy phenols even further compared to unloaded catalysts. However, the formation of light phenols was suppressed, leading to further loss of yield. This could be a direct influence of reduction in active surface area due to Na_2CO_3 loading leading to charring.

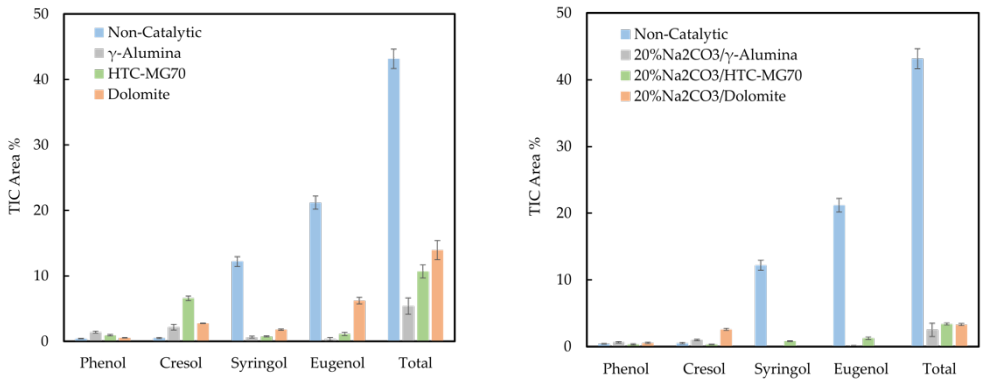

Figure 9. (**a**) Effect of support catalysts and (**b**) Na_2CO_3-loaded catalysts on Phenolics.

4. Conclusions

γ-Alumina, HTC-MG70 and dolomite were compared with Na_2CO_3-loaded γ-alumina, HTC-MG70 and dolomite on its influence on beechwood pyrolysis vapors. In general, the application of these catalysts drastically reduced the multifunctional oxygenates generated during pyrolytic decomposition and enhanced the formation of moderately deoxygenated compounds.

HTC-MG70 was found to be the most effective in moderately deoxygenating the pyrolysis vapors amongst the support catalysts investigated in this research. For example, high oxygen-containing furfural was transformed to furan and furan-2-methyl. Further, the phenolic yield was drastically reduced and the analysis showed that the formation of light phenols was enhanced. Acids were considerably reduced, anhydro-sugars were completely removed and aromatic hydrocarbons were generated. Moreover, most notably, the application of HTC-MG70 sharply increased the content of linear ketones and methylated cyclopentanones. On the other hand, dolomite showed similar composition with an exception of not promoting formation of hydrocarbons. γ-alumina performed the least well as it retained the acids and other high oxygen-containing oxygenates. The inference that the HTC-MG70 was the most effective support catalyst was on the basis of higher relative TIC area % of hydrocarbons produced and reduction in the majority of the oxygen-containing compounds. This effectiveness of HTC can be attributed to its high specific surface area and the synergy between acid and basic sites. In contrast, the acidic nature of γ-alumina promoted the formation of high oxygen-containing furfural and it also did not show an impact on reducing the acids.

In the context of Na_2CO_3 loading, Na_2CO_3 on γ-alumina had a noticeable effect on eliminating more or less all the acids, enhancing the mono-oxy-ketones and producing

lighter furans. In contrast, Na_2CO_3 loading on dolomite and hydrotalcite did not showcase a major influence on the composition except for further enhancing the mono-oxy-ketones (e.g., acetone and cyclopentenones) and suppressing the formation of hydrocarbons. The clear impact of the Na_2CO_3/γ-alumina on deoxygenation is a result of uniform dispersion of the Na_2CO_3 particles on the γ-alumina, as evident from XRD analysis. The TGA analysis also revealed that the Na_2CO_3 was modified in the presence of γ-alumina creating other active sites. In contrast, the Na_2CO_3 incorporation onto the surface HTC seems to have not been modified, as it was detected in the XRD analysis. Further, the Na_2CO_3 on dolomite drastically reduced the specific surface area and this is probably the cause for no major impact of the Na_2CO_3 loading.

In summary, this research showed that the support catalysts such as hydrotalcite and dolomite can transform the complex mixture of oxygenates generated during pyrolysis into a mixture of intermediate compounds with lower oxygen content. Na_2CO_3 loading was necessary on γ-Al_2O_3 to produce a moderately deoxygenated composition. Interestingly, these intermediate compounds can undergo C-C coupling, hydrodeoxygenation, hydrogenation reactions for conversion into a wide range of hydrocarbon liquid fuels as mentioned in the literature. This also means that hydrogen (H_2) consumption in the downstream hydrodeoxygenation (HDO) process can be possibly reduced as a result of moderate in-situ deoxygenation. The quantification of stability/reusability of these catalysts can be a future topic of investigation.

Author Contributions: Conceptualization, H.M.P. and E.A.B.; data curation, H.M.P., formal analysis, H.M.P.; funding acquisition, E.A.B. and G.B.; investigation, H.M.P.; methodology, H.M.P. and E.A.B.; project administration, E.A.B. and G.B.; resources, E.A.B. and G.B.; supervision, E.A.B. and G.B.; validation, H.M.P.; visualization, H.M.P.; writing—original draft, H.M.P.; writing—review and editing, E.A.B. and G.B. All authors have read and agreed to the published version of the manuscript.

Funding: This project is funded by "Rijksdienst voor Ondermend", The Netherlands.

Institutional Review Board Statement: Not applicable.

Informed Consent Statement: Not applicable.

Data Availability Statement: Not applicable.

Acknowledgments: The authors would like to convey their gratitude to Bert Geerdink (University of Twente, Enschede) for his co-operation and support during the experiments. The authors would also like to thank K. Altena-Schildkamp (University of Twente, Enschede) for BET measurements. This research was performed within the EnCat project (Enhanced catalytic fast pyrolysis of biomass for maximum production of high-quality biofuels), within ERA-NET Bioenergy the ERA-NET Bioenergy, for which the authors are very grateful. We gratefully acknowledge the "Rijksdienst voor Ondermend Nederland" for funding the project "Encat".

Conflicts of Interest: The authors declare no conflict of interest.

References

1. Guo, M.; Song, W.; Buhain, J. Bioenergy and biofuels: History, status, and perspective. *Renew. Sustain. Energy Rev.* **2015**, *42*, 712–725, doi:10.1016/j.rser.2014.10.013.
2. Slade, R.; Bauen, A.; Gross, R. Global bioenergy resources. *Nat. Clim. Chang.* **2014**, *4*, 99–105, doi:10.1038/nclimate2097.
3. Nanda, S.; Mohammad, J.; Reddy, S.N.; Kozinski, J.A.; Dalai, A.K. Pathways of lignocellulosic biomass conversion to renewable fuels. *Biomass Convers. Biorefinery* **2013**, *4*, 157–191, doi:10.1007/s13399-013-0097-z.
4. Singh, R.; Krishna, B.B.; Mishra, G.; Kumar, J.; Bhaskar, T. Strategies for selection of thermo-chemical processes for the valorisation of biomass. *Renew. Energy* **2016**, *98*, 226–237, doi:10.1016/j.renene.2016.03.023.
5. Limayem, A.; Ricke, S.C. Lignocellulosic biomass for bioethanol production: Current perspectives, potential issues and future prospects. *Prog. Energy Combust. Sci.* **2012**, *38*, 449–467, doi:10.1016/j.pecs.2012.03.002.
6. Leibbrandt, N.; Knoetze, J.; Gorgens, J. Comparing biological and thermochemical processing of sugarcane bagasse: An energy balance perspective. *Biomass Bioenergy* **2011**, *35*, 2117–2126, doi:10.1016/j.biombioe.2011.02.017.
7. Bridgwater, A. Principles and practice of biomass fast pyrolysis processes for liquids. *J. Anal. Appl. Pyrolysis* **1999**, *51*, 3–22, doi:10.1016/s0165-2370(99)00005-4.

8. Bridgwater, A. Review of fast pyrolysis of biomass and product upgrading. *Biomass Bioenergy* **2012**, *38*, 68–94, doi:10.1016/j.biombioe.2011.01.048.
9. French, R.; Czernik, S. Catalytic pyrolysis of biomass for biofuels production. *Fuel Process. Technol.* **2010**, *91*, 25–32, doi:10.1016/j.fuproc.2009.08.011.
10. Jaea, J.; Tompsett, G.A.; Foster, A.J.; Hammond, K.; M.Auerbachac, S.; Lobo, R.F.; Huber, G.W. Investigation into the shape selectivity of zeolite catalysts for biomass conversion. *J. Catal.* **2011**, *279*, 257–268, doi:10.1016/j.jcat.2011.01.019.
11. Mihalcik, D.J.; Mullen, C.; Boateng, A.A. Screening acidic zeolites for catalytic fast pyrolysis of biomass and its components. *J. Anal. Appl. Pyrolysis* **2011**, *92*, 224–232, doi:10.1016/j.jaap.2011.06.001.
12. Hernando, H.; Hernández-Giménez, A.M.; Ochoa-Hernández, C.; Bruijnincx, P.C.A.; Houben, K.; Baldus, M.; Pizarro, P.; Coronado, J.M.; Fermoso, J.; Čejka, J.; et al. Engineering the acidity and accessibility of the zeolite ZSM-5 for efficient bio-oil upgrading in catalytic pyrolysis of lignocellulose. *Green Chem.* **2018**, *20*, 3499–3511, doi:10.1039/c8gc01722k.
13. Asadieraghi, M.; Daud, W.M.A.W.; Abbas, H.F. Heterogeneous catalysts for advanced bio-fuel production through catalytic biomass pyrolysis vapor upgrading: A review. *RSC Adv.* **2015**, *5*, 22234–22255, doi:10.1039/c5ra00762c.
14. Hernando, H.; Jiménez-Sánchez, S.; Fermoso, J.; Pizarro, P.; Coronado, J.M.; Serrano, D.P. Assessing biomass catalytic pyrolysis in terms of deoxygenation pathways and energy yields for the efficient production of advanced biofuels. *Catal. Sci. Technol.* **2016**, *6*, 2829–2843, doi:10.1039/c6cy00522e.
15. Nokkosmäki, M.; Kuoppala, E.; Leppämäki, E.; Krause, A. Catalytic conversion of biomass pyrolysis vapours with zinc oxide. *J. Anal. Appl. Pyrolysis* **2000**, *55*, 119–131, doi:10.1016/s0165-2370(99)00071-6.
16. Kalogiannis, K.; Stefanidis, S.; Karakoulia, S.; Triantafyllidis, K.; Yiannoulakis, H.; Michailof, C.; Lappas, A. First pilot scale study of basic vs acidic catalysts in biomass pyrolysis: Deoxygenation mechanisms and catalyst deactivation. *Appl. Catal. B Environ.* **2018**, *238*, 346–357, doi:10.1016/j.apcatb.2018.07.016.
17. Lin, Y.; Zhang, C.; Zhang, M.; Zhang, J. Deoxygenation of Bio-oil during Pyrolysis of Biomass in the Presence of CaO in a Fluidized-Bed Reactor. *Energy Fuels* **2010**, *24*, 5686–5695, doi:10.1021/ef1009605.
18. Lu, Q.; Zhang, Z.-F.; Dong, C.-Q.; Zhu, X.-F. Catalytic Upgrading of Biomass Fast Pyrolysis Vapors with Nano Metal Oxides: An Analytical Py-GC/MS Study. *Energies* **2010**, *3*, 1805–1820, doi:10.3390/en3111805.
19. Stefanidis, S.; Kalogiannis, K.; Iliopoulou, E.; Lappas, A.; Pilavachi, P. In-situ upgrading of biomass pyrolysis vapors: Catalyst screening on a fixed bed reactor. *Bioresour. Technol.* **2011**, *102*, 8261–8267, doi:10.1016/j.biortech.2011.06.032.
20. Yathavan, B.K.; Agblevor, F.A. Catalytic Pyrolysis of Pinyon–Juniper Using Red Mud and HZSM-5. *Energy Fuels* **2013**, *27*, 6858–6865, doi:10.1021/ef401853a.
21. Imran, A.; Bramer, E.A.; Seshan, K.; Brem, G. High quality bio-oil from catalytic flash pyrolysis of lignocellulosic biomass over alumina-supported sodium carbonate. *Fuel Process. Technol.* **2014**, *127*, 72–79, doi:10.1016/j.fuproc.2014.06.011.
22. Nguyen, T.; Zabeti, M.; Lefferts, L.; Brem, G.; Seshan, K. Conversion of lignocellulosic biomass to green fuel oil over sodium based catalysts. *Bioresour. Technol.* **2013**, *142*, 353–360, doi:10.1016/j.biortech.2013.05.023.
23. Xue, X.; Pan, Z.; Zhang, C.; Wang, D.; Xie, Y.; Zhang, R. Analysis of Bio-Oil Derived from Catalytic Pyrolysis of Pine Sawdust over Sodium Salts-Supported γ-Al 2 O 3. *Environ. Prog. Sustain. Energy* **2019**, *38*, doi:10.1002/ep.13174.
24. Levin, D.B.; Chahine, R. Challenges for renewable hydrogen production from biomass. *Int. J. Hydrog. Energy* **2010**, *35*, 4962–4969, doi:10.1016/j.ijhydene.2009.08.067.
25. Rogers, K.A.; Zheng, Y. Selective Deoxygenation of Biomass-Derived Bio-oils within Hydrogen-Modest Environments: A Review and New Insights. *ChemSusChem* **2016**, *9*, 1750–1772, doi:10.1002/cssc.201600144.
26. Veses, A.; Aznar, M.; Martínez, I.; Martinez, J.D.; López, J.; Navarro, M.V.; Callén, M.; Murillo, R.; García, T. Catalytic pyrolysis of wood biomass in an auger reactor using calcium-based catalysts. *Bioresour. Technol.* **2014**, *162*, 250–258, doi:10.1016/j.biortech.2014.03.146.
27. Ly, H.V.; Lim, D.-H.; Sim, J.W.; Kim, S.-S.; Kim, J. Catalytic pyrolysis of tulip tree (Liriodendron) in bubbling fluidized-bed reactor for upgrading bio-oil using dolomite catalyst. *Energy* **2018**, *162*, 564–575, doi:10.1016/j.energy.2018.08.001.
28. Islam, W. A review of dolomite catalyst for biomass gasification tar removal. *Fuel* **2020**, *267*, 117095, doi:10.1016/j.fuel.2020.117095.
29. Lee, C.H.; Choi, S.W.; Yoon, H.J.; Kwon, H.J.; Lee, H.C.; Jeon, S.G.; Lee, K.B. Na2CO3-doped CaO-based high-temperature CO2 sorbent and its sorption kinetics. *Chem. Eng. J.* **2018**, *352*, 103–109, doi:10.1016/j.cej.2018.06.141.
30. Zeng, H.-Y.; Feng, Z.; Deng, X.; Li, Y.-Q. Activation of Mg–Al hydrotalcite catalysts for transesterification of rape oil. *Fuel* **2008**, *87*, 3071–3076, doi:10.1016/j.fuel.2008.04.001.
31. Hora, L.; Kelbichová, V.; Kikhtyanin, O.; Bortnovskiy, O.; Kubička, D. Aldol condensation of furfural and acetone over MgAl layered double hydroxides and mixed oxides. *Catal. Today* **2014**, *223*, 138–147, doi:10.1016/j.cattod.2013.09.022.
32. Dou, B.; Wang, C.; Song, Y.; Chen, H.; Jiang, B.; Yang, M.; Xu, Y. Solid sorbents for in-situ CO2 removal during sorption-enhanced steam reforming process: A review. *Renew. Sustain. Energy Rev.* **2015**, *53*, 536–546, doi:10.1016/j.rser.2015.08.068.
33. Yeo, T.Y.; Ashok, J.; Kawi, S. Recent developments in sulphur-resilient catalytic systems for syngas production. *Renew. Sustain. Energy Rev.* **2018**, *100*, 52–70, doi:10.1016/j.rser.2018.10.016.
34. Kuśtrowski, P.; Chmielarz, L.; Bożek, E.; Alsawalha, M.; Roessner, F. Acidity and basicity of hydrotalcite derived mixed Mg–Al oxides studied by test reaction of MBOH conversion and temperature programmed desorption of NH3 and CO2. *Mater. Res. Bull.* **2003**, *39*, 263–281, doi:10.1016/j.materresbull.2003.09.032.

35. Min, Y.J.; Hong, S.-M.; Kim, S.H.; Lee, K.B.; Jeon, S.G. High-temperature CO2 sorption on Na2CO3-impregnated layered double hydroxides. *Korean J. Chem. Eng.* **2014**, *31*, 1668–1673, doi:10.1007/s11814-014-0116-1.
36. Schröder, E. Experiments on the pyrolysis of large beechwood particles in fixed beds. *J. Anal. Appl. Pyrolysis* **2004**, *71*, 669–694, doi:10.1016/j.jaap.2003.09.004.
37. Zhou, R.-S.; Snyder, R.L. Structures and transformation mechanisms of the η, γ and θ transition aluminas. *Acta Crystallogr. Sect. B Struct. Sci.* **1991**, *47*, 617–630, doi:10.1107/s0108768191002719.
38. Eschenbacher, A.; Saraeian, A.; Jensen, P.A.; Shanks, B.H.; Li, C.; Duus, J..; Smitshuysen, T.E.L.; Damsgaard, C.D.; Hansen, A.B.; Kling, K.I.; et al. Deoxygenation of wheat straw fast pyrolysis vapors over Na-Al2O3 catalyst for production of bio-oil with low acidity. *Chem. Eng. J.* **2020**, *394*, 124878, doi:10.1016/j.cej.2020.124878.
39. Lu, Q.; Li, W.-Z.; Zhu, X.-F. Overview of fuel properties of biomass fast pyrolysis oils. *Energy Convers. Manag.* **2009**, *50*, 1376–1383, doi:10.1016/j.enconman.2009.01.001.
40. Patwardhan, P.R.; Brown, R.C.; Shanks, B.H. Product Distribution from the Fast Pyrolysis of Hemicellulose. *ChemSusChem* **2011**, *4*, 636–643, doi:10.1002/cssc.201000425.
41. Sun, G.; Li, Y.; Cai, Z.-Z.; Teng, Y.; Wang, Y.; Reaney, M.J. K 2 CO 3 -loaded hydrotalcite: A promising heterogeneous solid base catalyst for biolubricant base oil production from waste cooking oils. *Appl. Catal. B: Environ.* **2017**, *209*, 118–127, doi:10.1016/j.apcatb.2017.02.078.
42. Luo, Z.; Wang, S.; Liao, Y.; Cen, K. Mechanism Study of Cellulose Rapid Pyrolysis. *Ind. Eng. Chem. Res.* **2004**, *43*, 5605–5610, doi:10.1021/ie030774z.
43. Shen, D.; Gu, S. The mechanism for thermal decomposition of cellulose and its main products. *Bioresour. Technol.* **2009**, *100*, 6496–6504, doi:10.1016/j.biortech.2009.06.095.
44. Mante, O.D.; Rodriguez, J.A.; Senanayake, S.; Babu, S.P. Catalytic conversion of biomass pyrolysis vapors into hydrocarbon fuel precursors. *Green Chem.* **2015**, *17*, 2362–2368, doi:10.1039/c4gc02238f.
45. Ghalibaf, M.; Doddapaneni, T.R.K.C.; Alén, R. Pyrolytic behavior of lignocellulosic-based polysaccharides. *J. Therm. Anal. Calorim.* **2018**, *137*, 121–131, doi:10.1007/s10973-018-7919-y.
46. Zhou, X.; Li, W.; Mabon, R.; Broadbelt, L.J. A mechanistic model of fast pyrolysis of hemicellulose. *Energy Environ. Sci.* **2018**, *11*, 1240–1260, doi:10.1039/c7ee03208k.
47. Nowakowski, D.; Bridgwater, T.; Elliott, D.; Meier, D.; de Wild, P. Lignin fast pyrolysis: Results from an international collaboration. *J. Anal. Appl. Pyrolysis* **2010**, *88*, 53–72, doi:10.1016/j.jaap.2010.02.009.